Electronic Supplementary Material (ESI) for Environmental Science: Nano.

The pH, time, and size dependency of silver nanoparticle dissolution: the road to equilibrium

Bastiaan Molleman and Tjisse Hiemstra*

Supporting information

(19 pages, 10 figures, 1 table)

*Corresponding author's email address: **tjisse.hiemstra@wur.nl**
Phone: +31 317 48 2342; Fax: +31 317 41 9000
Department of Soil Quality, Wageningen University
P.O. Box 47, 6700 AA Wageningen, the Netherlands

S1 Solubility of silver oxide

The solubility of Ag_2O (s) has been studied by a large number of authors. These experiments have been evaluated by Biedermann and Sillén.[1] The solubility reaction of Ag_2O (s) can be given as:

$$\tfrac{1}{2}\ Ag_2O\ (s) + \tfrac{1}{2}\ H_2O\ (l) \Leftrightarrow Ag^+\ (aq) + OH^-\ (aq) \text{ with } \log K = -7.71$$

The same solubility product has been reported more recently by Duro et al.,[2] although they incorrectly refer to it as silver hydroxide (AgOH). The solubility diagram of Ag_2O (s) is given below.

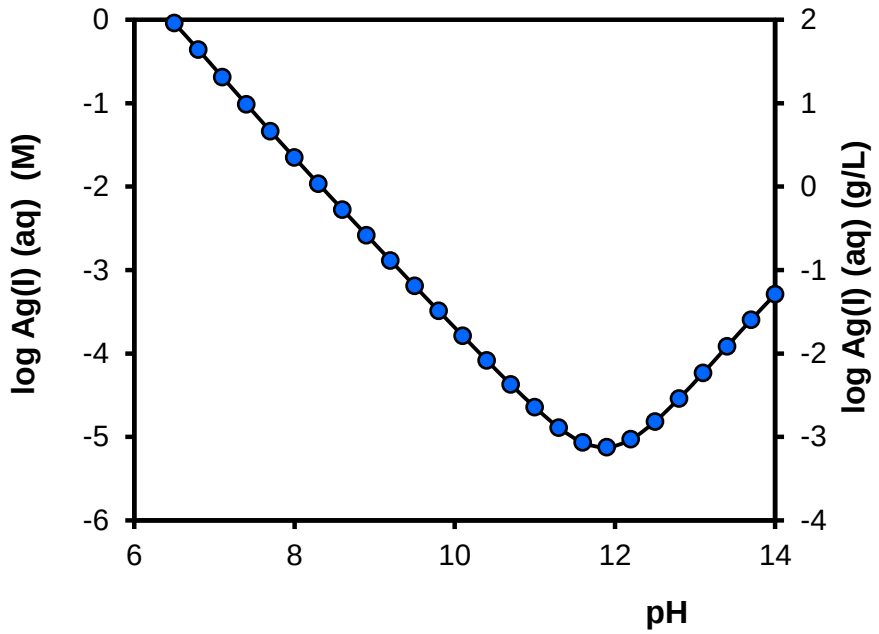

Fig. S1 pH-dependent solubility of Ag_2O(s). At the left y-axis, the unit is in mol/L. At the right y-axis, the unit is g/L.

The calculation show a solubility of 1 mol L^{-1} of Ag^+ at about pH 6.5., i.e. silver oxide can be very soluble. At pH 7, the solubility is 0.2 mol L^{-1} or more than 20 g Ag L^{-1}. If the solubility of Ag_2O(s) is tested in water and the pH is left free, the solubility is about a factor 1000 times less. The reason is the strong increase of the pH as a result of the dissolution process, releasing OH^- ions. A pH of about 10.1 is reached and the corresponding solubility is near 20 mg L^{-1} of Ag.

S2 Particle size distribution of NanoComposix AgNPs

In our article, we use the mean diameter and specific surface area (A_P) as provided by NanoComposix. Fig. S2 gives the particle size distributions for $AgNP_5$, $AgNP_{10}$ and $AgNP_{20}$ as extracted from the material data sheets provided with the product. The figure shows which percentage of particles falls into the different size categories. The dotted lines represent normal distributions having the mean and standard deviation given by the manufacturer.

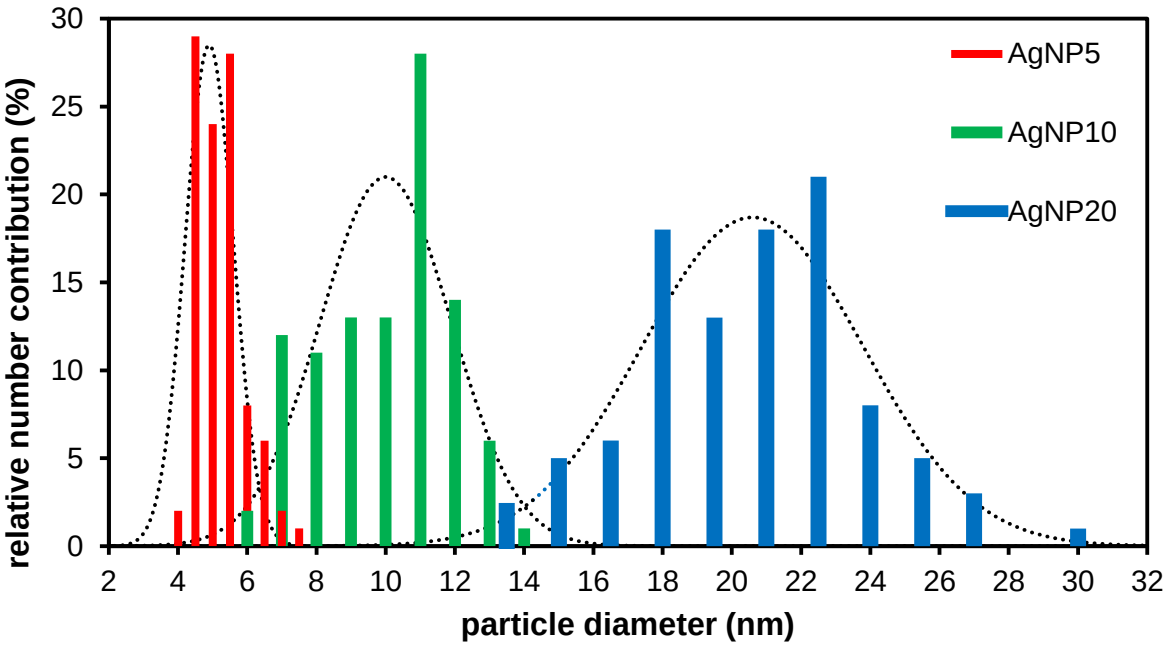

Fig. S2 Particle size distributions for $AgNP_5$, $AgNP_{10}$, and $AgNP_{20}$ as given by the manufacturer. Relative abundance is based on individual counts. Dotted lines are calculated with a normal distribution function using 4.9 ± 0.7, 9.9 ± 1.9, 20.6 ± 3.2, respectively, and corrected for the size intervals (0.5, 1.0, and 1.5, respectively).

The A_P provided by NanoComposix was calculated from the relative abundance of particle diameters assuming spherical particles. Deviation from the spherical shape will increase the specific surface area. The effect for oblate (lens-shaped) and prolate (egg-shaped) particles has been calculated below showing that A_P increases with less than 10% if one of the axes is 20% longer or shorter. Given that the great majority of particles appear well rounded in the TEM photographs (provided by NanoComposix), we feel that no correction for non-ideal shape is needed.

Specific surface area of spheroids

A flattened spheroid, having an equatorial radius, a, longer than the polar radius, c, is known as oblate or lens-shaped. The surface area for oblate particles, A_{ob}, can be calculated using:

$$A_{\mathrm{ob}} = 2\pi a^2\left(1 + \frac{1-e^2}{e}\tanh^{-1} e\right) \text{ where } e = \sqrt{1 - \frac{c^2}{a^2}}$$

An elongated spheroid, having a polar radius (c) longer than the equatorial radius (a) is known as prolate or egg-shaped. The surface area for prolate particles, A_{pro}, can be calculated using:

$$A_{\mathrm{pro}} = 2\pi a^2\left(1 + \frac{1-e^2}{e}\tanh^{-1} e\right) \quad \text{where } e = \sqrt{1 - \frac{a^2}{c^2}}$$

The volume of a spheroid is equal to:

$$V = \frac{4}{3}\pi a^2 \mathrm{c}$$

Note that for a perfect sphere with a = c = r, the latter equation reduces to the well-known equation for the volume of a sphere.

Using these formulae we find that for oblate particles with c up to 20% shorter than a, A_{P} is no more than 10% larger than for a sphere with r equal to a. Similarly, we find that for a prolate spheroid with c up to 20% longer than a, A_{P} is no more than 5% larger than for a sphere with r equal to the average of c and a.

S3 Two methods of sample preparation compared

The pH and time dependency of the Ag^+ release have been tested using two different experimental methods. In short, samples for method I were mixed in a single large batch, and then divided up into several sets of duplicates. At each sampling time, one set of duplicates was taken and analyzed destructively. Duplicates for method II were individually mixed, but not divided into sets. At each sampling time, solution was taken from the same batches. The experimental setups are explained in more detail in Material and Methods of the main text.

Ag^+ release for both experimental setups were compared and found to yield very similar results (see Figure S3). After 1 day, Ag^+ release is almost exactly similar, after 1 and 2 weeks, method II shows a somewhat lower dissolution, but after 5 weeks, this difference has almost completely disappeared.

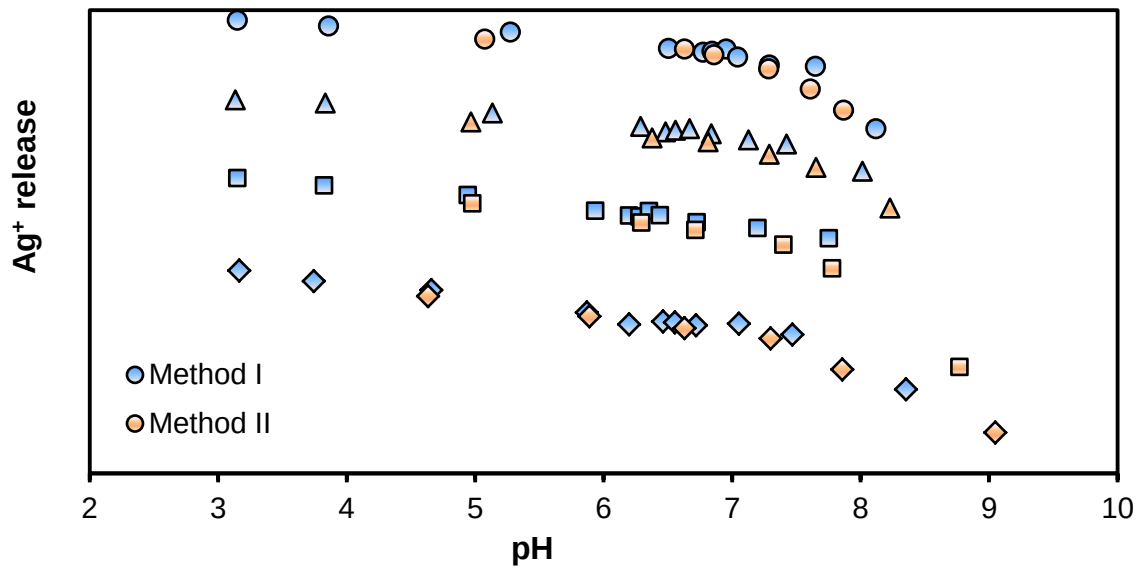

Fig. S3 Ag^+ release measured using the two different experimental setups. Data is plotted on a logarithmic scale, and data points of a single time-step have been multiplied with 10^x for clarity. Therefore, this graph does not(!) represent the progression of dissolution, but serves to compare the results between the two different methods at one (!) sampling time. From top to bottom data points represent Ag^+ release after 5 weeks (circles), 2 weeks (triangles), 1 week (squares), and 1 day (diamonds).

S4 Effect of shaking on AgNP dissolution

During preliminary experiments, it was observed, that a silver coating was formed on the wall of the sample containers. The silver deposit was visible only in those regions which were intermittently exposed to the sample and air as a result of the shaking motion. This led us to suspect that shaking may cause AgNPs to precipitate out of solution. We reasoned that, similarly to bubbles forming in a soapy suspension, the effect might not occur in a stationary sample. In this work, we have therefore chosen for an unconventional experimental method where samples are not agitated.

Theoretical considerations

With a mass density of $10.5 \cdot 10^6$ g m^{-3}, a 5 nm spherical AgNP will have a mass of about $7 \cdot 10^{-19}$ g. At a solid to solution ratio of ~ 10 mg L^{-1}, or 10 g m^{-3}, this means approximately $7 \cdot 10^{-20}$ m^3 of solution is available to each particle, which translates to a sphere with a diameter of roughly 500 nm. The maximum travel distance between an oxygen molecule and the particle surface is thus ~ 250 nm. For a 20 nm AgNP, this distance is 4 times larger, or approximately 1 µm.

For the simplified case of 1-dimensional diffusion, the root mean-square distance of diffusion, $\sqrt{\overline{x^2}} = \sqrt{2Dt}$, can be used to estimate the distance over which the concentration becomes roughly uniform in time, t. At room temperature, or 298 K, dissolved oxygen has a diffusion coefficient, D, of $2.1 \cdot 10^{-9}$ m^2 s^{-1}, leading to a 1 second diffusion length of around $\sqrt{\overline{x^2}} = 6.5\ 10^{-5}$ m or 65 µm. Although this is a simplified view, the diffusion length in 1 second is greatly exceeds the distance between particles. Therefore, from the perspective of diffusion, shaking the samples will not influence the Ag^+ release kinetics on the timescale that we used.

Experimental

To test empirically that shaking does not limit AgNP dissolution, we compared the Ag^+ release found in the preliminary experiments (with shaking for 3 weeks) to the Ag^+ release found in our final experiments (without shaking). Slightly larger AgNPs were used for the preliminary experiment ($AgNP_6$, 5.7 ± 1.0 nm) than for the final experiment

($AgNP_5$, 4.9 ± 0.7). The pH dependency of Ag^+ release at high pH is shown for both experiments in Fig. S4.

When the dissolution is expressed per unit surface area, a clear difference is found (Fig. S4). This could be due to the use of particles of different size or could be due to our shaking versus non-shaking procedure. If due to a difference in size, the Ag^+ release of the 5.7 nm AgNP is expected to be lower because large particles are more stable. The data can be explained assuming a slightly larger size (7 nm), which could be in line with our observation of the formation of a silver film that may increase the mean particle size in the system in case of shaking. Whatever, we may safely conclude based on the theoretical considerations and the above experimental observations that our procedure without shaking cannot have led to underestimation of the Ag^+ release compared to a standard procedure with continuously shaking. On the contrary, shaking may induce deviations.

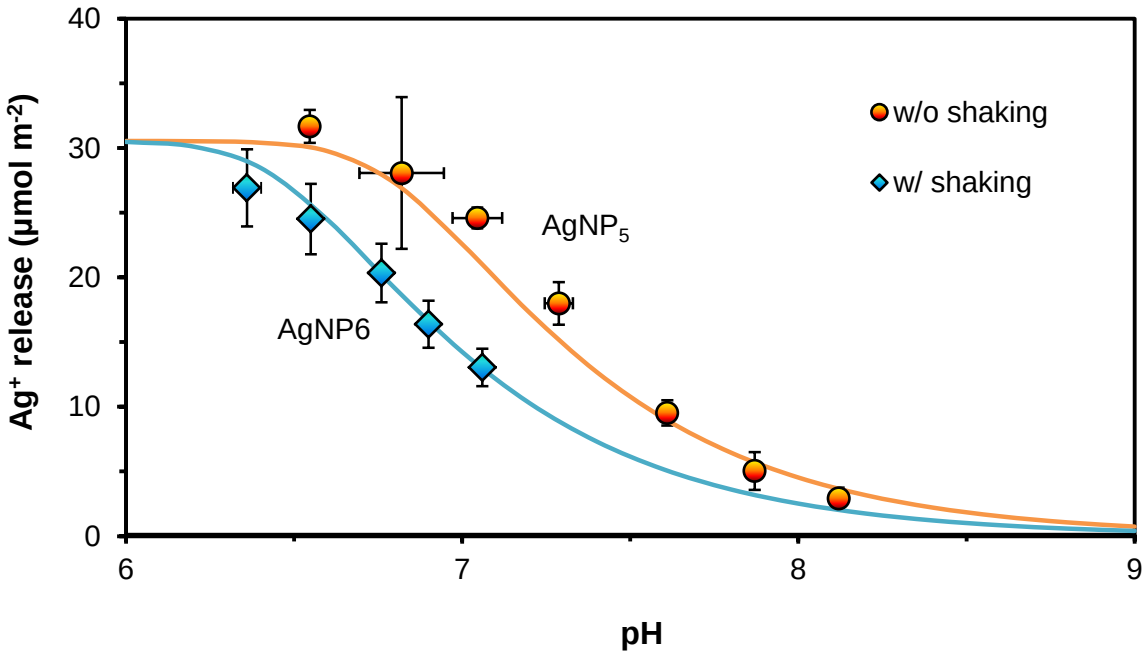

Fig. S4 pH dependent Ag^+ release curves for $AgNP_5$ (without shaking, circles) and $AgNP_6$ (with shaking, diamonds). The $AgNP_6$ data were obtained in a preliminary experiment without duplicates, the error bars represent a ~ 10% error. The transparent symbols are calculated from the $AgNP_6$ data, under the assumption that 15 % precipitated out of solution forming a silver film with negligible contribution to AT and thus to the Ag^+ release equilibrium. Dotted lines represent the model description of the data using a fitted $\log K^0_{H/Ag}$ value.

S5 Ag^+ retention by ultrafiltration filter units

To determine the dissolved Ag^+ concentrations in our samples, the AgNPs were separated from the solution using Microsep™ Advance Centrifugal Devices (3 kDa). The ultrafiltration membrane in the filter units is made of polyether sulfone, which may adsorb Ag^+. This may lead to a lower Ag^+ concentration in the filtrate than in the sample. To compensate for the Ag^+ retention, a volume of sample was filtrated to saturate the filtration membrane; this first filtrate was discarded. A second volume was filtered to obtain a filtrate with Ag^+ concentrations equal to those in the sample.

This method to obtain accurate Ag^+ concentrations was tested for $AgNO_3$ solutions with three different background electrolytes (1 mM): $NaHCO_3$ (pH ~8), $NaNO_3$ (pH ~ 5.5) and HNO_3 (pH ~ 3). UPW was centrifuged over the filter units 3 times before the first sample was introduced. Fig. S5 shows Ag^+ concentrations determined by ICP-MS before and after filtration. Both the first and the second filtrate are analyzed for Ag^+ concentrations. At pH 8, the ultrafiltration units are seen to retain a significant amount of Ag^+, presumably by binding to reactive groups in the filtration membrane. This is supported by the low retention at lower pH values. At concentration levels relevant to the experimentation ($[Ag^+] > 0.1$ μM), the second filtrate is seen to contain Ag^+ at levels adequately close to the unfiltered sample. Results obtained using this method can thus be considered as representative for the Ag^+ concentrations in the sample.

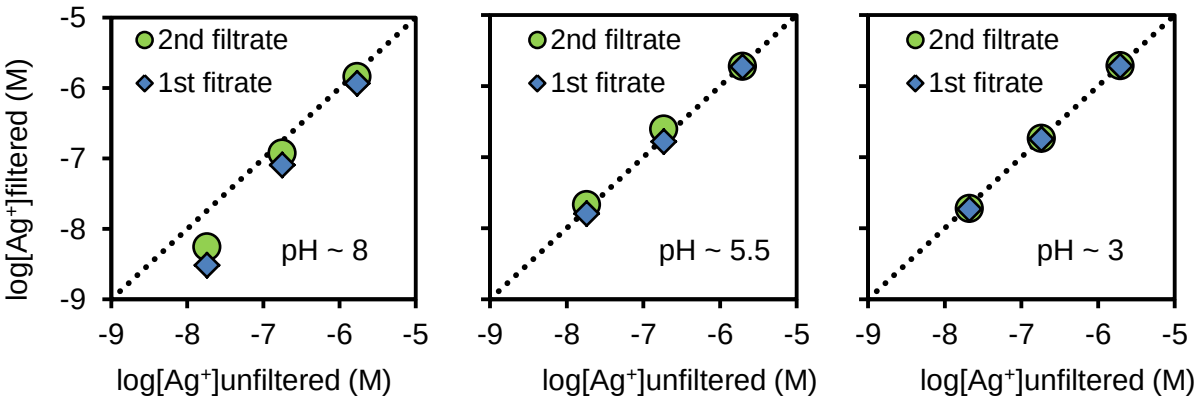

Fig. S5 Ag^+ concentrations in the first and second filtrate plotted against Ag^+ concentrations in unfiltered samples in 1 mM solutions of $NaHCO_3$ (pH ~ 8), $NaNO_3$ (pH ~ 5.5), and HNO_3 (pH ~ 3). As results show, the Ag^+ concentration found in the second filtrate is very close or equal to that found in the unfiltered samples at concentrations above 10^{-7} M.

S6 Ag^+ release at a linear scale

As mentioned in the text, the largest contribution to total release of Ag^+ occurs at low pH. Dissolution in the neutral pH range has the most important impact on the Ag^+ concentrations with respect to the reaction quotient, Q (see main text), but contributes only marginally to total Ag^+ release. When plotted on a linear scale, as in Fig. S6, the magnitude of Ag^+ release at low pH is immediately apparent. Especially for the larger particles, Ag^+ release is strongly enhanced at low pH, reaching up to 9 equivalent atomic Ag layers, whereas dissolution at neutral to high pH is mostly limited to the first atomic layer.

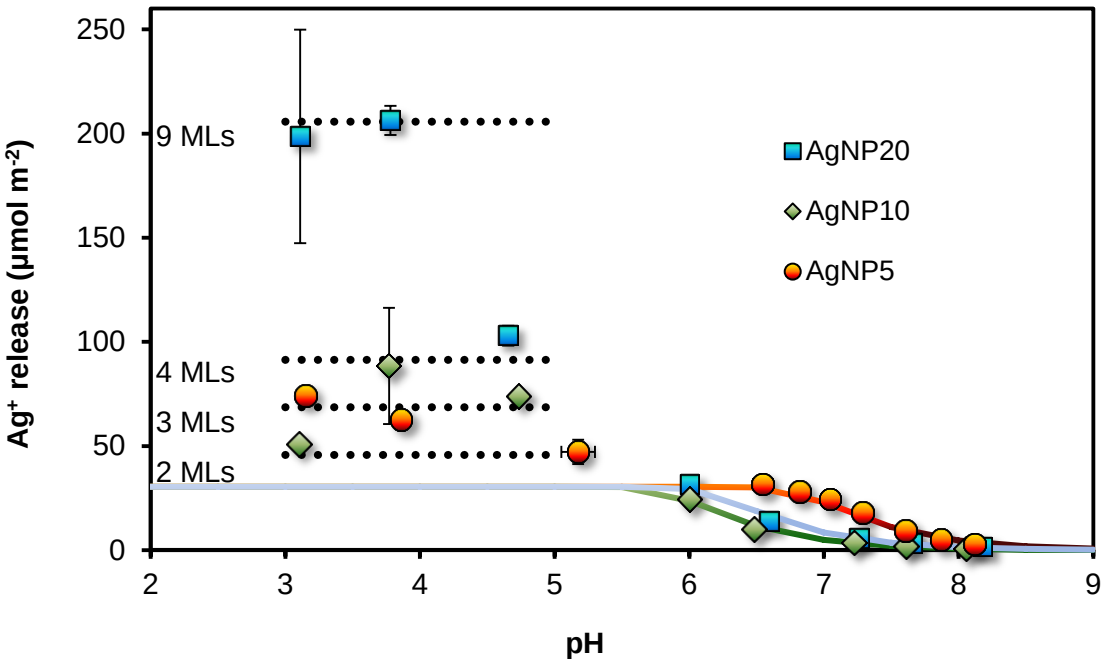

Fig. S6 The pH dependency of Ag^+ release on a linear scale, together with the expected release at dissolution of a multitude of Ag monolayers (MLs). With a Ag-Ag distance of 0.2889 nm,[3] a Ag density of ~ 14 nm^{-2} is found on the hexagonally organized [111] face. Dissolution of a single layer of Ag atoms thus releases 23 µmol m^{-2}. The figure shows that at neutral to high pH, less than 2 MLs are dissolved, while at low pH up to 9 MLs can be released as Ag^+.

S7 Possible surface structures

Oxidation states of the AgNP surface

Silver at the surface of AgNPs is only partially oxidized.[4] Two different states of oxidation can be found at the surface of AgNP. Under mildly oxidized conditions, the valence of Ag at the surface can be represented by z_{Ag} = +⅓ v.u. At the [111] faces of icosahedral AgNP, subvalency leads to a surface structure with ≡Ag_3OH groups with a density of 4.6 nm^{-2}.[5]

A higher surface oxidation state can be reached by formation of subvalent silver over multiple layers. Subvalent silver organized in two layers can be found in solids such as Ag_6O_2,[6] Ag_2F,[7] and Ag_2NiO_2.[8]

For the gas-solid interface, oxidation over multiple atomic layers may occur when metallic silver is exposed to atomic oxygen at high temperature.[9] According to our bond valence analysis of the reported structures, this leads to full oxidation (z_{Ag} = +1 v.u.) in the first layer and subvalency (z_{Ag} = +½ v.u.) in the second layer.

For the water-solid interface, formation of subvalent silver over two layers has been suggested in case of strong oxidation. Formation of Ag_6O octahedra has been proposed in our previous contribution.[5] However, present attempts to optimize the geometry of such a Ag_6O structure using MO-DFT pointed to a large instability of the oxygen ion in hexa-coordination with six subvalent silver ions. To reconcile the presence of a higher oxidation state with the formation of subvalent silver over two layers without formation of Ag_6O octahedra, we suggest a new surface structure.

Oxidation of Ag over multiple layers is structurally possible, if Ag at the surface is partially replaced by oxygen ions. The oxygens in this position are able to coordinate to three underlying silver leading to the formation ≡Ag_3OH with a subvalency of z_{Ag} = +⅓ v.u. for the three Ag ions in the subsurface. Simultaneously, the remaining surface atoms can also attain a subvalent state by partial oxidation. Depending on the precise surface structure, ≡Ag_2OH or ≡Ag_3OH may form having a subvalency of z_{Ag} = +½ v.u. or z_{Ag} = +⅓ v.u., respectively. The result is OH groups on top of as well as in between the atoms of the outer silver layer, leading to subvalency in both the surface and the subsurface.

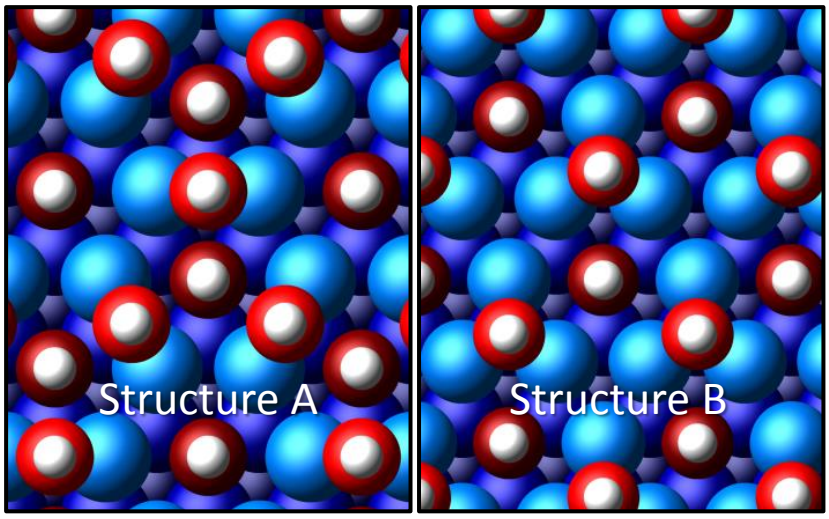

Fig. S7 Geometric representations of the [111] face of silver nanoparticles with partially oxidized, i.e. subvalent, silver coordinated to OH groups. Oxidation occurs over two layers leading to the formation of subvalent $\equiv Ag_3OH$ (z_{Ag} = +⅓ v.u.) in the subsurface. Structure A can be formed without surface restructuring at removal of the original $\equiv Ag_3OH$ if this group has coordinated to an underlying single Ag atom that is simultaneously removed. Structure B can only be formed if restructuring of the surface occurs. Formation of structures A and B results in a Ag^+ release of 31 and 29 μmol m^{-2}, respectively, in agreement with the model applied in Fig. 2 of the main text.

Possible surface structures

Figure S7 shows two typical surface structures with subvalency over two layers. In both structures, the deeper lying OH groups coordinate to three silver atoms in the subsurface. A higher subvalency arises in the surface than in the subsurface, resulting in a gradual transition between completely oxidized Ag^+ in solution to fully reduced metallic Ag^0 in the AgNP core.

Structure A (Fig. S7a) can be directly formed at oxidation of a $\equiv Ag_3OH$ site if it coordinates to a single underlying Ag atom, forming a silver tetrahedron topped with a hydroxide ($\equiv AgAg_3OH$). If the underlying Ag is removed upon oxidation of a tetrahedral $\equiv Ag_3OH$ site, the resulting opening in the second layer of silver can be occupied by an oxygen atom, allowing partial oxidation of the underlying Ag atoms in the third layer. The above process leads to the formation of new $\equiv Ag_3OH$ sites ($z_{Ag} = +⅓$ v.u.) from subsurface, Ag^0. The remaining silver at the surface transforms into $\equiv Ag_2OH$ surface groups ($z_{Ag} = +½$ v.u.). Structure A can be represented with the stoichiometric notation $\equiv Ag_5(OH)_2$. Formation of structure A requires the release of four Ag^+ ions, or $x + z = 4$, resulting in a maximum Ag^+ release of 31 μmol m^{-2}.

In structure B (Fig. S7b), both the surface and the subsurface have only ≡Ag_3OH sites. In contrast to structure A, one in four atoms in the subsurface does not coordinate to a hydroxide anion, and may be regarded as metallic. Overall, the silver in this structure is thus less oxidized, with an average subvalence of $\bar{z}_{Ag} = +¼$ v.u. in the subsurface, and $z_{Ag} = +⅓$ v.u. in the surface groups. Structure B can only be formed by moving Ag ions to new lattice positions; the necessary restructuring may be possible in case of high surface mobility.[10] Structure B has the stoichiometric notation ≡$Ag_{4.5}(OH)_{1.5}$ and $x + z = 3.75$, leading to a maximum Ag^+ release of 29 μmol m^{-2}.

S8 Effect of multiple particle sizes on dissolution

In this work, a correlation was found between the overall specific surface area (A_{P}) and the values of $\log K^{0}_{\mathrm{H/Ag}}$ that best described the observed Ag^{+} release. This suggests that within batches, the particle size distribution (see Fig. S2) also results in a distribution of surface stabilities. If the chemical heterogeneity resulting from the particle size distribution is large enough, it could affect the slope, $\Delta\log[Ag^{+}]/\Delta\mathrm{pH}$. The effect of a distribution of surface stabilities has been investigated by modelling Ag^{+} release for polydisperse and monodisperse nanoparticle suspensions.

Modelling approach

Monodisperse suspensions were simulated using the value for A_{P} given by the manufacturer and a AgNP concentration of 10 mg L^{-1}; $\log K^{0}_{\mathrm{H/Ag}}$ values were calculated using the relation:

$$\log K^{0}_{\mathrm{H/Ag}} = 0.08\, A_{\mathrm{P}} + 5.2$$

as was found by linear regression (main text) from the data generated in this work as well as collected data from literature.[11, 12]

In simulations of polydisperse suspensions, for each size category, k, an individual AgNP concentration was defined, as well as individual values for A_{P} and $\log K^{0}_{\mathrm{H/Ag}}$. Relative number contributions, $f_{N,k}$, for the different size categories were extrapolated directly from the particle size distributions for $AgNP_5$, $AgNP_{10}$, and $AgNP_{20}$ (Fig. S2) and transformed into relative mass contributions, $f_{M,k}$, using:

$$f_{M,k} = f_{N,k} {d_k}^3 / \sum f_{N,k} {d_k}^3$$

where d_k is the average diameter of particles in each category. The mass concentration of AgNPs was obtained by multiplying $f_{M,k}$ with the overall AgNP concentration used in the simulation of the monodisperse suspension.

The specific surface area for spherical particles of a specific size, $A_{\mathrm{P},k}$ is given by:

$$A_{\mathrm{P},k} = \frac{6000}{\pi d_k \rho_{\mathrm{Ag}}}$$

with d_k in nm and a mass density, ρ_{Ag}, equal to that of bulk silver (10.49 g cm^{-3}). The individual $\log K^0_{\mathrm{H/Ag}}$ values are calculated as for the monodisperse suspensions.

Simulated results

The results of both simulations for $AgNP_5$, $AgNP_{10}$, and $AgNP_{20}$ are shown in Fig. S8. The dotted lines represent polydisperse suspensions, the solid lines monodisperse. The graph shows that the slope of the polydisperse suspensions is slightly lower than that of the monodisperse suspensions, as suspected in the case of chemical heterogeneity. However, the difference is small, showing that the size distributions of these AgNPs are sufficiently narrow that results can be modelled with a single surface stability constant. It is expected, however, that AgNPs with a wider size distribution, will have a greater chemical heterogeneity, and using a single $\log K$ value may no longer suffice.

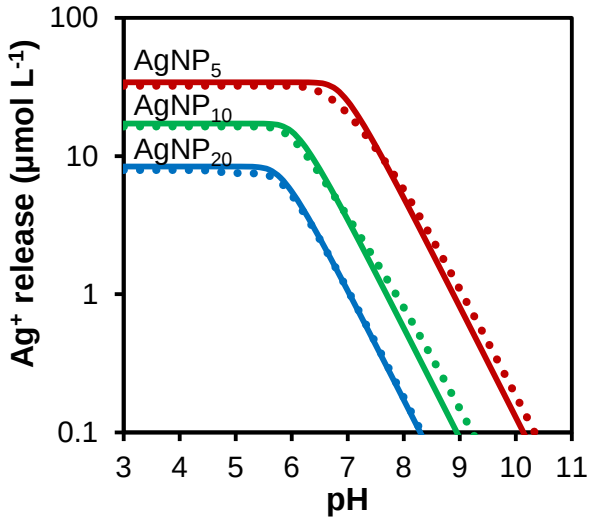

Fig. S8 Simulations of Ag^+ release in monodisperse (full lines) and polydisperse (dotted lines) nano-suspensions with average particle diameters of 5, 10, and 20 nm. In monodisperse suspensions, all particles have the same $\log K^0_{\mathrm{H/Ag}}$ value, whereas particles with different $\log K^0_{\mathrm{H/Ag}}$values are defined in the polydisperse suspensions. For the polydisperse systems, we have used the particle size distribution as reported by NanoComposix (see Fig. S2).

S9 Linking the empirical model to the surface structure

In this work, we have analyzed both the equilibrium Ag^+ concentrations and the kinetics of Ag^+ release. From both perspectives, the results suggest that two different processes are active. Equilibrium concentrations suggest that a surface-based dissolution process controls the Ag^+ concentrations at high pH. The mechanistic surface structural model, for which the theoretical base has been laid in our earlier publication,[5] can be refined to accurately describe the data. At low pH, data suggest that a different, more heterogeneous process is active. The time dependency of the Ag^+ release has been analyzed using first order kinetics as a premise. This empirical approach points to two independent sources of Ag^+ release: a fast pool, active below pH ~7, and a slow pool, active at pH < 8. As shown in Fig. S9, the size of the slow pool is nearly identical to the dissolution profile of the surface structural model, suggesting that they represent the same process.

The above strongly suggests that the Ag^+ source identified as the slow pool is the surface structure which is slowly reaching equilibrium. This shows that Ag^+ release due to surface equilibration can be distinguished from dissolution at low pH, based on kinetics as well as on equilibrium concentrations. The fact that the slow pool identified by analyzing kinetics matches the surface structural model so closely, suggests that our surface structures may closely match the actual AgNP surface.

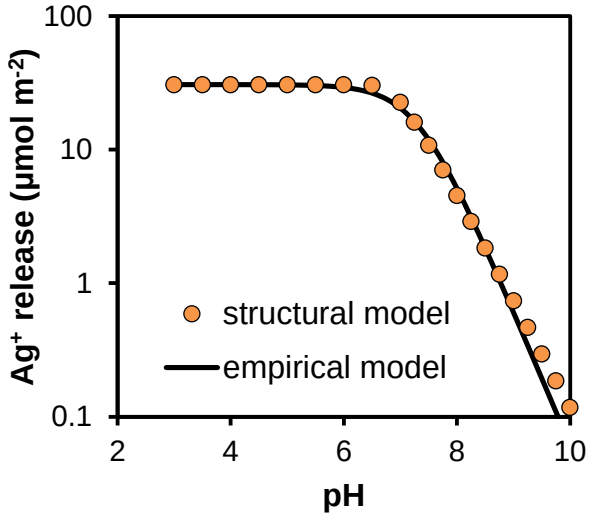

Fig. S9 Model predictions of Ag^+ release due to equilibration of the surface structure compared to the size of the slow pool. The strong similarity between both sources suggests that they represent the same process.

S10 Data by Adamczyk et al.

We have applied our final kinetic modelling to data available in literature; notably, short-term data provided by Adamczyk et al.[11] We have simulated their data using a single set of parameters which adequately describes Ag^+ release for three AgNP concentrations at pH 3.5, as well as for a single AgNP concentration at pH 6.2 (see Fig. S10). This is a notable improvement over modeling efforts by Adamzcyk et al.,[11] who have not defined pH as an input parameter and therefore needed to define separate models for the two pH values.

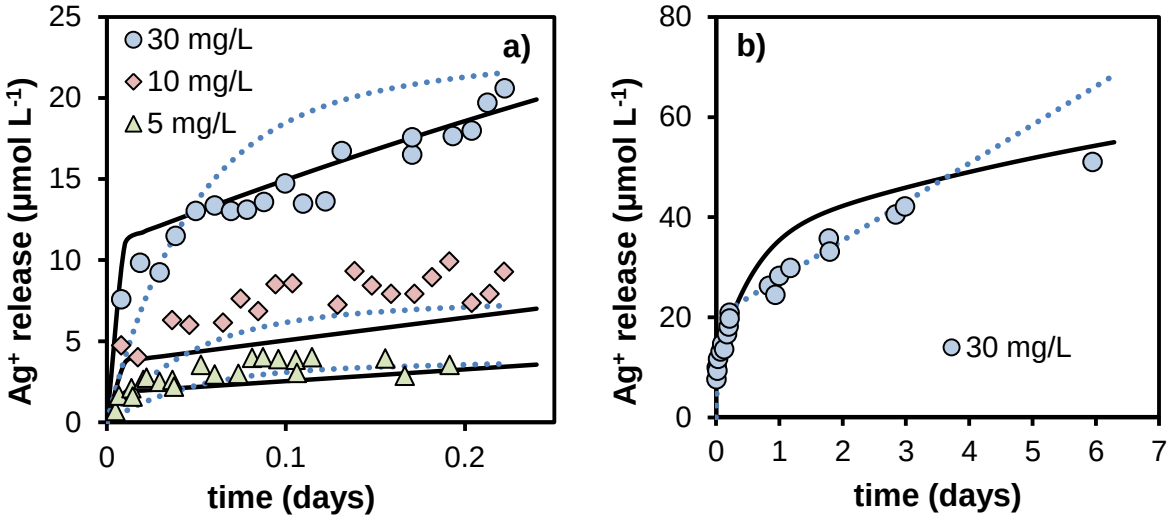

Fig. S10 Ag^+ release data by Adamzcyk et al.[11] at pH 3.5, measured for three different AgNP concentrations on short timescales (a) and for a single AgNP concentration on a longer timescale (b). Model lines represent our own final model (full lines) and the model developed by Adamzcyk et al.[11] using the parameters they present as their best fit (dotted lines).

Our model captures a number of striking trends, which can be observed in the data. The high release that occurs at the very beginning of the experiment (Fig. S10a) is well described and is due to the near instantaneous oxidative release of surface sites with adsorbed molecular oxygen, i.e. $\equiv Ag_3OH\text{-}O_2$ sites. This is followed by a slower rate of release, which in our model is the result of stripping of patches. At even longer timescales (after ~ 2 days), Ag^+ release is even slower (see Fig. S10b). At this point, undersaturation has strongly decreased due to AgNP dissolution, and patch-wise release has run its course. The ongoing release can be attributed to equilibration of the surface, which is slow as a result of the rate-limiting step of oxygen adsorption to the surface. In

accordance with the data, our model predicts that the system, even at these acid conditions, will reach eventually reach equilibrium. It can be seen that the model formulated by Adamzcyk et al.[11] assumes continuous dissolution of the AgNPs without reaching any equilibrium. This assumption provides good data description on the mid-term (1 - 3 days, see Fig. S10b), but is clearly seen to fail on the longer term.

Parameterization

A few of the parameters, as optimized for our own data, need to be adjusted in order to obtain the best possible data description.

The rate constant for oxygen adsorption on the AgNP surface, k_{ads}, has been increased two-fold. As the rate constant for desorption, k_{ads}, remained unchanged, the equilibrium constant, $K^{*}_{\mathrm{O}_2}$, is also increased twofold. This also implies that rate limitation by a low value for θ_2 occurred at a later stage. These differences may be related to the presence of citrate in our systems, which may compete for binding sites, thus reducing the surface loading with oxygen.

Furthermore, the rate constants for oxidation and reduction, k_{ox} and k_{red} have both been adapted resulting in a lower value for the equilibrium constant ($\Delta\log K = 6$). It implies that the AgNP material used by Adamczyk et al.[11] has a larger stability towards oxidation. This is expected since the particles are larger and this finding is in line with our data and those of Peretyazhko et al.[12], as shown in Fig. 3b of the main text.

Finally, patch-wise release plays a considerably smaller role in the experiments by Adamczyk et al.[11] than in our own experiments. Patch-wise release is highly variable between the various particles used in our experiments, but the trend is that larger particles release proportionally more Ag^{+} through this process. The fact that patch-wise release is relatively unimportant for these 12 nm AgNPs may, again, be related to the absence of capping agents. As we show in Fig. 5 (main text), AgNPs with a higher surface tension on the edges of the theoretical disk-like depletion islands, have a larger critical diameter for patch nucleation at the same undersaturation. Here, the interesting implication is that citrate may thus stabilize AgNPs at circum-neutral conditions, where the surface equilibrium dominates, whereas it stimulates patch-wise release.

References

1. G. Biedermann and L. G. Sillén, *Acta Chemica Scandinavica*, 1960, 14, 717-725.
2. L. Duro, M. Grivé, E. Cera, C. Domènech and J. Bruno, *Update of a thermodynamic database for radionuclides to assist solubility limits calculation for performance assessment*, 2006.
3. I. K. Suh, H. Ohta and Y. Waseda, *Journal of Materials Science*, 1988, 23, 757-760.
4. A. Henglein, *Chemistry of Materials*, 1998, 10, 444-450.
5. B. Molleman and T. Hiemstra, *Langmuir*, 2015, 31, 13361-13372.
6. W. Beesk, P. G. Jones, H. Rumpel, E. Schwarzmann and G. M. Sheldrick, *Journal of the Chemical Society, Chemical communications*, 1981, 664-665.
7. H. Ott and H. Seyfarth, *Zeitschrift für Kristallographie-Crystalline Materials*, 1928, 67, 430-433.
8. M. D. Johannes, S. Streltsov, I. I. Mazin and D. I. Khomskii, *Physical Review B*, 2007, 75, 180404(R).
9. N. M. Martin, S. Klacar, H. Grönbeck, J. Knudsen, J. Schnadt, S. Blomberg, J. Gustafson and E. Lundgren, *The Journal of Physical Chemistry C*, 2014, 118, 15324-15331.
10. J. Sun, L. He, Y. C. Lo, T. Xu, H. Bi, L. Sun, Z. Zhang, S. X. Mao and J. Li, *Nature Materials*, 2014, 13, 1007-1012.
11. Z. Adamczyk, M. Oćwieja, H. Mrowiec, S. Walas and D. Lupa, *Journal of Colloid and Interface Science*, 2016, 469, 355-364.
12. T. S. Peretyazhko, Q. Zhang and V. L. Colvin, *Environ. Sci. Technol.*, 2014, 48, 11954-11961.